NASA Technical Memorandum 101473
ICOMP-89-3

Numerical Computation of Shock Wave—Turbulent Boundary Layer Interaction in Transonic Flow Over an Axisymmetric Curved Hill

S.-W. Kim
Institute for Computational Mechanics in Propulsion
Lewis Research Center
Cleveland, Ohio

February 1989

NASA

NUMERICAL COMPUTATION OF SHOCK WAVE - TURBULENT BOUNDARY LAYER INTERACTION IN TRANSONIC FLOW OVER AN AXISYMMETRIC CURVED HILL

S.-W. Kim*
Institute for Computational Mechanics in Propulsion
Lewis Research Center
Cleveland, Ohio 44135

Summary

A control-volume based finite difference computation of a turbulent transonic flow over an axisymmetric curved hill is presented. The numerical method is based on the SIMPLE algorithm, and hence the conservation of mass equation is replaced by a pressure correction equation for compressible flows. The turbulence is described by a k-ε turbulence model supplemented by a near-wall turbulence model. In the method, the dissipation rate in the region very close to the wall is obtained from an algebraic equation and that for the rest of the flow domain is obtained by solving a partial differential equation for the dissipation rate. The other flow equations are integrated up to the wall. It is shown that the present turbulence model yields the correct location of the compression shock. The other computational results are also in good agreement with experimental data.

---

*Work funded under Space Act Agreement C99066G.

Nomenclature

A_u	coefficient for axial velocity correction equation
A_v	coefficient for radial velocity correction equation
A_1	constant coefficient for f_μ equation (=0.025)
A_2	constant coefficient for f_μ equation (=0.00001)
A_ϵ	constant coefficient for f_ϵ equation
c_ℓ	turbulence model constants for ϵ equation, (ℓ=1,2)
$c_{\mu f}$	constant coefficient for eddy viscosity equation (=0.09)
f_μ	wall damping function for eddy viscosity equation
f_ϵ	wall damping function for ϵ_w equation
k	turbulent kinetic energy
k_e	effective thermal conductivity ($=k_m+k_t$)
k_m	thermal conductivity
k_t	turbulent thermal conductivity ($=C_p\mu_t/\sigma_T$)
p	pressure
P_r	production rate of turbulent kinetic energy
R	gas constant.
R_t	turbulent Reynolds number ($=k^2/(\nu\epsilon_1)$)
r	radial coordinate
T	temperature
u	Reynolds averaged velocity in axial direction
u_τ	friction velocity ($=\sqrt{(\tau_w/\rho)}$)
$\overline{u'v'}$	Reynolds stress
V	velocity vector ($=\{u,v\}$)
v	Reynolds averaged velocity in radial directions
x	axial coordinate
y	normal distance from the wall

y^+	wall coordinate ($=u_\tau y/\nu$)
ϵ	dissipation rate
ϵ_1	dissipation rate of turbulent kinetic energy
ϵ_w	dissipation rate inside the near-wall layer
κ	von Karman constant (=0.41)
μ	molecular viscosity
μ_e	effective viscosity ($=\mu+\mu_t$)
μ_t	turbulent viscosity
ν	kinematic viscosity of fluid
ν_t	turbulent eddy viscosity
ρ	density
σ_k	turbulent Prandtl number for k-equation
σ_T	turbulent Prandtl number for energy equation
σ_ϵ	turbulent Prandtl number for ϵ-equation
τ_w	wall shearing stress
Φ	dissipation function for energy equation

Superscripts

*	current value
'	incremental (or corrective) value
^	non-dimensional value normalized by the free stream value

Mathematical symbol

$\sum$	summation

Introduction

The transonic flow over an axisymmetric curved hill [1] has received considerable attention in recent years as a bench mark test case to assess the capability of numerical methods as well as turbulence models to be used as design/analysis tools for fluid machinery. In the numerical calculation of turbulent transonic flows, prediction of the correct pressure field depends on the location of the shock and the location of the shock depends on the viscous force development. Therefore, emphasis was laid upon selecting and/or developing a suitable turbulence model in References 2 and 3. The turbulence models tested in these references ranged from algebraic turbulence models to two-equation turbulence models, and varying degrees of success have been obtained.

The transonic flow calculation presented herein constitutes one of the earliest applications of the newly developed numerical method [4] as well as the turbulence model [5]. These are described below.

The control-volume method based on the SIMPLE algorithm [6,7] is mostly used to solve incompressible flows the domain of which can be discretized by an orthogonal mesh. Due to their strongly convergent nature, pressure correction methods have been used extensively to solve complex turbulent flows including chemically reacting turbulent flows [8-9]. The numerical method used herein is an extension of the pressure correction method to solve incompressible as well as compressible flows with arbitrary, complex geometries. The compressible flow equations are mostly solved by flux splitting methods. The Beam-Warming method [10] and the McCormack method [11] are representatives of the flux splitting methods. The flux splitting methods have originally been developed to solve the Euler equations and then extended to include the viscous term to solve the

Navier-Stokes equations. The most distinguished difference between the two classes of methods lies in the way the diffusion term is treated. In the pressure correction methods, the diffusion term is incorporated into the stiffness matrix while, in the flux splitting methods, the diffusion term is incorporated into the system of equations as the load vector term. For turbulent flows with extensive recirculation zones, the pressure correction methods may be numerically more stable than the other class of methods, conceptually; however, the pressure correction methods have mostly been used for incompressible flows and the flux splitting methods have mostly been used for compressible flows. Therefore, definitive advantages and disadvantages of these two classes of methods can not be discussed with confidence as yet.

A few papers to extend the SIMPLE method to solve compressible flows have appeared in recent years [4,12-14]. Some difficulties have been encountered in the course of these studies. A fully staggered grid layout was used in the original SIMPLE method to solve flow equations using orthogonal meshes [6,7]. In many flow problems of practical importance, the boundary geometries are complex and arbitrary shaped blockages may exist inside the flow path. One difficulty was identifying a suitable grid layout to solve the Navier-Stokes equations defined on complex geometries. In Reference 12, a collocated grid layout was used and an artificial dissipation was included to prevent velocity-pressure decoupling. In Reference 15, a fully staggered grid layout for incompressible flows was used and the velocity vector was located at all grid points except at the pressure grid point, hence the number of degrees of freedom for velocities is doubled and that of pressure remains the same as in the original case. In References 4 and 14, the velocities were located at the same grid points

and the pressure was located at the centroid of the four adjacent velocity grid points. This grid layout has been used successfully in the penalty finite element method for a long time [16]. It was first used in the control-volume based finite difference method by Vanka et. al. [17]. They mentioned that it was not easy to obtain convergent solutions due to velocity-pressure decoupling. The mechanism that leads to the velocity-pressure decoupled solution was heuristically shown in Reference 15. In Reference 14, the velocity-pressure decoupling was eliminated by using a non-conforming domain for mass imbalance calculation. In Reference 4, the velocity-pressure decoupling was eliminated by treating the pressure correction equation as a standard partial differential equation rather than treating it as a constraint condition. In the method, the off-diagonal terms were moved to the load vector term and the resulting system of equations was solved using the tri-diagonal matrix algorithm (TDMA). Thus any uncertainty that may arise due to the use of a non-conforming domain for mass imbalance calculation does not exist in the present method [4].

Another difficulty was identifying the most suitable numerical procedure for pressure correction. The SIMPLE-R [6], the SIMPLE-C [18], and the standard SIMPLE algorithm [6] were used in References 13, 14, and 4, respectively. The pressure, velocity, and density were corrected based on the incremental pressure (or pressure correction) in References 13 and 14. In Reference 4, only the pressure and velocity were corrected from the incremental pressure. Density was obtained from the equation of state for a perfect gas so that the same numerical procedure could be equally applicable for numerical computation of chemically reacting turbulent flows in the future. The numerical procedure for pressure correction, especially for compressible flows, may need to be further studied in the future.

The accuracy and the convergence nature of the numerical method used herein has been tested by solving a class of example flow cases. The example problems considered in Reference 4 include: a developing channel flow, a developing pipe flow, a two-dimensional laminar flow in a 90 degree bent channel, polar cavity flows, and a turbulent supersonic flow over a compression ramp. It was found that the numerical method used herein yielded accurate computational results even when highly skewed, unequally spaced, curved grids were used. It is also found that the present method was strongly convergent for high Reynolds number flows as well as for flows with complex geometries.

In numerical calculations of turbulent flows, the near-wall region has been incorporated into the numerical analyses usually by using the wall functions [19], two- or multi-layer turbulence models [20-22], and low Reynolds number turbulence models [23].

The most widely used wall function methods have been derived from the logarithmic velocity profile based on the experimental observation that the turbulence in the near-wall region can be described in terms of the wall shearing stress. The wall function methods are not valid if the logarithmic velocity profile no longer prevails in the near-wall region. Such cases include separated and/or reattaching flows, unsteady flows, flows over surfaces with mass injection and/or suction, and near-wall low turbulent Reynolds number flows.

In the two- or multi-layer turbulence models, the turbulence in the near-wall layer has been described by algebraic equations. In some of these turbulence models [20,21], the turbulent kinetic energy and the dissipation rate in the near-wall layer have been constructed by piecewise continuous functions. As a consequence, the computational results may depend on the

location of the partition between the near-wall layer and the fully turbulent region. In Reference 20, a quadratic variation of the turbulent kinetic energy has been assumed in the near-wall region and the dissipation rate has been derived from the logarithmic velocity profile equation. The underlying assumption that the turbulent kinetic energy grows in proportion to the square of the distance from the wall in the near-wall region is also questionable, since the quadratic variation of the turbulent kinetic energy is valid only inside the viscous sublayer and becomes invalid as the fully turbulent region is approached.

In the low Reynolds number turbulence models, the high Reynolds number turbulence models have been extended to include the near-wall low turbulence effect [23]. In this class of methods, the near-wall low turbulence effects have been incorporated into the high Reynolds number turbulence models by using wall damping functions. These wall damping functions have been derived mostly from numerical experiments in such a way that the low Reynolds number turbulence models could approximately reproduce the experimentally observed turbulent flow phenomena in the near-wall region. In this class of methods, a significant number of grid points has to be assigned in the near wall region in order to resolve the stiff dissipation rate equation.

Aside from the above two classes of methods, a new approach has been used in Chen and Patel [24] to resolve the near-wall turbulence. In the method, only the turbulent kinetic energy equation of the k-ϵ turbulence model has been extended to include the near-wall low turbulence region and the dissipation rate inside the near-wall layer has been prescribed algebraically. The dissipation rate equation has been obtained from a k-equation turbulence model [25]. Thus the turbulent kinetic energy and the

dissipation rate vary smoothly from the wall toward the outside fully turbulent region. In this case, it would be more appropriate to classify this turbulence model as a partially low Reynolds number turbulence model to distinguish it from the other two classes of methods. Advantages of the partially low Reynolds number approach over the other methods can be summarized as follows. The turbulence in external flows and that in near-wall boundary layer flows have quite different length scales [26]. The turbulence length scale of the external flows is related to the flow field characteristics. On the other hand, the turbulence length scale of boundary layer flows is strongly related to the normal distance from the wall. This characteristic of the wall bounded turbulent flows can be described quite naturally by the partially low Reynolds number turbulence models. The same purpose could be achieved by the low Reynolds number turbulence models as more experimental data become available; however, the gradient of the dissipation rate is the most stiff in the near-wall region, and a great number of grid points has to be used in this region for the low Reynolds number turbulence models to resolve the dissipation rate. Therefore, the partially low Reynolds number turbulence models seem to be more advantageous as compared with the low Reynolds number turbulence models, unless the low Reynolds number turbulence models can describe the wall bounded turbulent flows more accurately.

The turbulence model used in this report belongs to the partially low Reynolds number turbulence models. Development of the near-wall turbulence model and its application to fully developed turbulent channel and pipe flows can be found in Reference 5. It has been shown in the reference that the present near-wall turbulence model can resolve the over-shoot phenomena of the turbulent kinetic energy and the dissipation rate in the region very

close to the wall and that significantly improved computational results for the turbulence structure in the near-wall region have been obtained. More application of the near-wall turbulence model for complex turbulent flows such as the supersonic flow over a compression ramp with shock wave - turbulent boundary layer interaction [27] can be found in Reference 4.

Reynolds Averaged Navier-Stokes Equations and Numerical Method

The compressible turbulent flow equations are given as;

$$\frac{\partial}{\partial x}(\rho u) + \frac{1}{r}\frac{\partial}{\partial r}(\rho r v) = 0. \tag{1}$$

$$\frac{\partial}{\partial x}(\rho u u) + \frac{1}{r}\frac{\partial}{\partial r}(\rho r v u) = \frac{\partial}{\partial x}(\tau_{xx}) + \frac{1}{r}\frac{\partial}{\partial r}(r\tau_{xr}) - \frac{\partial p}{\partial x} \tag{2}$$

$$\frac{\partial}{\partial x}(\rho u v) + \frac{1}{r}\frac{\partial}{\partial r}(\rho r v v) = \frac{\partial}{\partial x}(\tau_{rx}) + \frac{1}{r}\frac{\partial}{\partial r}(r\tau_{rr}) - \frac{\partial p}{\partial r} - \frac{\tau_{\theta\theta}}{r} \tag{3}$$

$$\frac{\partial}{\partial x}(\rho C_p u T) + \frac{1}{r}\frac{\partial}{\partial r}(\rho r C_p v T) = \frac{\partial}{\partial x}\left[k_e\frac{\partial T}{\partial x}\right] + \frac{1}{r}\frac{\partial}{\partial r}\left[r k_e\frac{\partial T}{\partial r}\right] + u\frac{\partial p}{\partial x} + v\frac{\partial p}{\partial r} + \Phi \tag{4}$$

where

$$\tau_{xx} = 2\mu_e\frac{\partial u}{\partial x} - \frac{2\mu_e}{3}(\nabla\cdot V),$$

$$\tau_{xr} = \tau_{rx} = \mu_e \left[\frac{\partial u}{\partial r} + \frac{\partial v}{\partial x} \right],$$

$$\tau_{rr} = 2\mu_e \frac{\partial v}{\partial r} - \frac{2\mu_e}{3} (\nabla \cdot \mathbf{V}),$$

$$\tau_{\phi\phi} = 2\mu_e \frac{v}{r} - \frac{2\mu_e}{3} (\nabla \cdot \mathbf{V}),$$

$$\Phi = \mu_e \left\{ 2\left[\frac{\partial u}{\partial x}\right]^2 + 2\left[\frac{\partial v}{\partial r}\right]^2 + 2\left[\frac{v}{r}\right]^2 + \left[\frac{\partial u}{\partial r} + \frac{\partial v}{\partial x}\right]^2 \right\} - \frac{2\mu_e}{3} (\nabla \cdot \mathbf{V})^2,$$

$$\nabla \cdot \mathbf{V} = \frac{\partial u}{\partial x} + \frac{1}{r} \frac{\partial (rv)}{\partial r},$$

and the density is obtained from the perfect gas law given as $p=\rho RT$. A turbulent Prandtl number (σ_T) of 0.75 was used for the energy equation, see the Nomenclature. The molecular viscosity and the thermal conductivity were obtained from the Sutherland's laws given as [28];

$$\frac{\mu}{\mu_o} = \left[\frac{T}{T_o}\right]^{3/2} \left[\frac{T_o + S}{T + S}\right] \tag{5}$$

where $\mu_o = 1.716 \times 10^{-5}$ Kg/m-sec, $T_o = 273.1^o$ Kelvin, $S = 110.6^o$ Kelvin; and

$$\frac{k_m}{k_o} = \left[\frac{T}{T_o}\right]^{3/2} \left[\frac{T_o + S}{T + S}\right] \tag{6}$$

where k_o = 0.0264 Kg/m-K, T_o = 273.1° Kelvin, and S = 194.4° Kelvin.

In the present method, all flow variables, except pressure, have been located at the same grid points and the pressure node has been located at the centroid of the cell. The control volume for the pressure correction equation is defined as the cell enclosed by the four neighboring grid points. Note that in the control-volume based finite difference methods, the discrete system of equations is derived by integrating the governing differential equations over the control volume [6]. For curvilinear grids, the required number of interpolations to obtain flow variables at the cell boundaries is significantly reduced by using the present grid layout. Enhanced convergence rate is partly attributed to the grid layout which required fewer interpolations [4].

The pressure correction equation for compressible flows is briefly discussed below for completeness. As in the standard pressure correction method, the density, the velocities, and the pressure are decomposed as;

$$\rho = \rho^* + \rho' \tag{7}$$

$$u = u^* + u', \tag{8}$$

$$v = v^* + v', \tag{9}$$

$$p = p^* + p' \tag{10}$$

The incremental pressure is related to the incremental density and the incremental velocities as;

$$p' = \rho' RT \tag{11}$$

$$u' = - A_u \frac{\partial p'}{\partial x} \tag{12}$$

$$v' = - A_v \frac{\partial p'}{\partial y} \tag{13}$$

where eq. (11) has been obtained from the equation of state; and eqs. (12) and (13) have been obtained from the discrete u- and v-momentum equations, respectively [4,6]. Substituting eqs. (7-13) into (1) yields, after some rearrangement;

$$\frac{\partial}{\partial x}\left[\frac{u^*}{RT} p'\right] + \frac{1}{r}\frac{\partial}{\partial r}\left[r\frac{v^*}{RT} p'\right] = \frac{\partial}{\partial x}\left[\rho^* A_u \frac{\partial p'}{\partial x}\right] + \frac{1}{r}\frac{\partial}{\partial r}\left[r\rho^* A_v \frac{\partial p'}{\partial r}\right] - \nabla\cdot(\rho^* \mathbf{V}) \tag{14}$$

where the last term in eq. (14) represents the mass imbalance. The incremental pressure is obtained by solving eq. (14), and the corresponding incremental velocities are obtained from eqs. (12-13). The flow variables are updated using eqs. (8-10), and these updated flow variables are used in computing the new current flow variables by solving eqs. (2-4) together with the turbulence equations. The iterative solution process is repeated until the mass imbalance in eq. (14) becomes negligible. In solving eq. (14), the off-diagonal terms in the discrete pressure correction equation were moved to the load vector term, and the resulting five diagonal system of equations was solved using the TDMA [4,6]. Even the slightest symptom of the velocity-pressure decoupling was not observed in the present flow case as well as for all the flow cases considered in Reference 4.

Turbulence Equations

A k-ϵ turbulence model supplemented with a near-wall turbulence model is described below. The turbulent kinetic energy equation for the entire flow domain is given as;

$$\frac{\partial}{\partial x}(\rho uk) + \frac{1}{r}\frac{\partial}{\partial r}(\rho rvk) = \frac{\partial}{\partial x}\left(\mu_e \frac{\partial k}{\partial x}\right) + \frac{1}{r}\frac{\partial}{\partial r}\left(r\mu_e \frac{\partial k}{\partial r}\right) + \rho P_r - \rho\epsilon \qquad (15)$$

where the production rate of turbulent kinetic energy (P_r) is the same as the dissipation function for the energy equation (Φ).

The dissipation rate inside the near-wall layer is given as;

$$\epsilon_w = \frac{\epsilon_1}{f_\epsilon} \qquad (16)$$

where

$$\left.\begin{aligned} \epsilon_1 &= \frac{c_\mu f^{3/4} k^{3/2}}{\kappa y} \\ f_\epsilon &= 1 - \exp(-A_\epsilon R_t) \\ R_t &= \frac{k^2}{\nu\epsilon_1} \\ A_\epsilon &= \frac{c_\mu f^{3/2}}{2\kappa^2} \end{aligned}\right\} \qquad (17)$$

Note that ϵ_1 in eq.(17) represents the standard dissipation rate for

near-wall turbulent flows in equilibrium state. The dissipation rate given as eq. (16) is used for eq. (15) in the near-wall region. For $y \approx 0$, eq. (16) takes the limit value given as $2\nu k/y^2$. Slightly away from the wall where the turbulence is in the equilibrium state, f_ϵ takes the unit value and eq. (16) becomes identical to eq. (17). The dissipation rate given as eq. (16) is formally identical to the one proposed by Wolfshtein [25]. The qualitatively similar dissipation rates used in the k-equation turbulence models of Gibson et. al. [29], Hassid and Poreh [30], and Acharya and Reynolds [31] can be written as;

$$\epsilon_w = c_\mu f^{3/4} f_{\epsilon h} \frac{k^{3/2}}{\kappa y} + \frac{2\nu k}{y^2} \tag{18}$$

where $f_{\epsilon h}$ is a wall damping function varying from zero on the wall to unity in the fully turbulent region. Note that the second term on the right hand side of eq. (18) can be obtained as an analytical solution of the turbulent kinetic energy equation for a limiting case as y approaches the wall. However, this term persists far out into the fully turbulent region, and hence eq. (16) has been preferred over eq (18), see Reference 5 for more discussion.

The dissipation rate for the rest of the flow domain is obtained by solving the convection-diffusion equation for the dissipation rate equation given as;

$$\frac{\partial}{\partial x}(\rho u \epsilon) + \frac{1}{r}\frac{\partial}{\partial r}(\rho r v \epsilon) = \frac{\partial}{\partial x}\left[\mu_e \frac{\partial \epsilon}{\partial x}\right] + \frac{1}{r}\frac{\partial}{\partial r}\left[r \mu_e \frac{\partial \epsilon}{\partial r}\right] + \rho c_1 \frac{P_r \epsilon}{k} - \rho c_2 \frac{\epsilon^2}{k} \tag{19}$$

The turbulence model constants used are given as: σ_k=0.75, σ_ϵ=1.15, c_1=1.39, and c_2=1.88. These turbulence model constants approximately satisfy the near-wall equilibrium turbulence condition and the decay rate of the grid turbulence observed in the experiment [32]. Further discussion on the establishment of these turbulence model constants can be found in References 33-34.

The eddy viscosity equation inside the near-wall layer is given as;

$$\nu_t = c_{\mu f} f_\mu \frac{k^2}{\epsilon_1} \tag{20}$$

where f_μ=1-exp($A_1\sqrt{R_t} + A_2 R_t^2$) . The wall damping function f_μ is a linear function of the distance from the wall in the viscous sublayer region and become unity in the fully turbulent region. The eddy viscosity given as eq. (20) grows in proportion to the cubic power of the distance from the wall. It can be found in References 5 and 23 that the near-wall analysis yields the same growth rate of the eddy viscosity in the region very close to the wall. The eddy viscosity in the rest of the flow domain is given as;

$$\nu_t = c_{\mu f} \frac{k^2}{\epsilon} \tag{21}$$

The domain for each differential equation is shown schematically in Figure 1 for clarity. For wall bounded turbulent flows, the equilibrium region extends from $y^+ \approx 30$ up to $y^+ \approx 300$. Thus the partition between the near-wall region and the fully turbulent outer region can be located between y^+ greater than 100 and less than 300 approximately.

Computational Results

The transonic flow considered in the present study is schematically shown in Figure 2. In the experiment [2], an axisymmetric circular-arc bump of thickness 1.9 cm and a chord length of 20.3 cm was attached at 60 cm downstream of a circular cylinder with the external diameter of 15.2 cm. The free stream Mach number was 0.875, the Reynolds number was 13.2×10^6/m, and the boundary layer thickness of the approaching transonic flow was 0.01 meters.

In the following calculations, the inlet boundary was located at one chord length upstream of the forward corner of the bump; and the exit boundary, at one chord length downstream of the rear end of the bump. Some degree of uncertainty that may be caused by numerical diffusion and inadequate grid size can always exist in any numerical analysis. To reduce the numerical uncertainty, a relatively fine grid (78 X 53) and a highly fine grid (108 X 65) have been used in the present study. The computational results obtained using these two grids differed by no more than a few percent. The computational results presented herein were obtained using the highly fine grid shown in Figure 3. The inlet boundary condition for the axial velocity and the turbulent kinetic energy were obtained from experimental data for a fully developed flat plate flow [35]. The non-dimensional velocity and the turbulent kinetic energy profiles were scaled to yield a boundary layer thickness of 0.01 meters at the inlet boundary. Uniform static pressure and uniform enthalpy were also prescribed at the inlet boundary. The no-slip boundary condition for velocities, a vanishing turbulent kinetic energy, and a constant temperature which corresponds to the free stream stagnation temperature were prescribed at

the solid wall boundary. The free stream flow condition was prescribed at the top boundary, and a vanishing gradient boundary condition was used for all flow variables at the exit boundary. The partition between the near-wall layer and the external region was located at approximately 5 percent of the boundary layer thickness away from the wall and 10 grid points were allocated inside the near-wall layer. The initial guess was obtained by extending the inlet boundary condition in the axial direction.

The discrete finite difference system of equations was solved iteratively until the error norms became smaller than the prescribed convergence criteria. Each iteration consisted of 7 sweeps of the pressure correction equation and 3 sweeps for the rest of the flow equations in the axial and in the radial directions, respectively. The pressure was updated using an under-relaxation factor of 0.57; and the rest of the flow variables, using an under-relaxation factor of 0.47. With the use of these under-relaxation parameters, divergence or convergence to an erroneous solution has not been encountered. The convergence criteria used were;

$$R_1 = \sum_{c=1}^{N_c} |\nabla\cdot(\rho\hat{\mathbf{V}})|_c < e_1 \tag{22}$$

$$R_2 = |(a_{i,j}^{n+1} - a_{i,j}^{n})/A_i^{n+1}| < e_2, \quad j=1,N, \tag{23}$$

where N_c is the number of pressure control volumes; the superscript n denotes the iteration level; the subscript i={u, v, p, T, k, ϵ} denotes each flow variable; the subscript j denotes each grid point; N denotes the number of degrees of freedom for each flow variable; and A_i denotes the maximum magnitude of the i-th flow variable. The iteration was terminated

when either eq. (22) or eq. (23) was satisfied. The converged solution was obtained after 750 iterations for $e_1=5x10^{-4}$ and $e_2=1x10^{-4}$. At the time of convergence R_1 and R_2 were approximately $4.5x10^{-4}$ and $1.1x10^{-4}$, respectively. The required computational time was approximately 11 minutes for the CRAY-XMP at NASA/LeRC.

The calculated iso-Mach lines are shown in Figure 4, where the incremental Mach number between the contour lines is 0.05. The static pressure contour lines are shown in Figure 5, where the pressure has been normalized by the inlet total pressure and the incremental pressure between the contour lines is 0.01. It can be seen from Figures 4 and 5 that the flow field is characterized by a relatively small supersonic pocket attached at the top of the curved hill. Neither the iso-Mach lines nor the pressure contour are available in References 1-3, and direct comparison of these contour lines with other computational results could not be made. The calculated static pressure on the wall is compared with experimental data as well as the numerical results of References 2 and 3 in Figure 6. It can be seen in the figure that the pressure distribution on the wall obtained by the McCormack method using Johnson's algebraic turbulence model [3] (hereafter abbreviated as J-A model) compares most favorably with experimental data. It is shown in the figure that the present turbulence model yielded significantly improved pressure distribution over the one [2] obtained by the McCormack method using the Wilcox-Rubesin Turbulence model (hereafter abbreviated as W-R model). It can also be seen in the Figure that the present turbulence model and the W-R model yielded a slightly more spread-out shock than the experimental data. In the present study, the computational results are compared mostly with those obtained using the W-R model [2] for the following reasons. Firstly, the k-ϵ class turbulence

models have wider applicability than the algebraic turbulence models, especially for turbulent flows through complex geometries. Secondly, the k-ϵ turbulence models seldom contain a flow-dependent adjustable constant; however, this is not always true for algebraic turbulence models [3]. And lastly, more extensive computational results for the present flow case, such as the flow separation and the turbulent kinetic energy profiles, were presented in Reference [2] than in Reference [3].

The streamline contour at the rear end of the hill is shown in Figure 7. The measure flow separation zone extended from x/c=0.7 to x/c=1.1, where c is the chord length. The present method yielded the flow recirculation zone extending from x/c=0.81 to x/c=1.12. The recirculation zone obtained in Reference 2 using the Cebeci-Smith turbulence model and the W-R model extended from x/c=0.81 to x/c=1.1 and from x/c=0.81 to x/c=1.2, respectively. It can be seen that these computational results exhibited decent comparison with the experimental data.

The mean velocity profiles at four axial locations are compared with experimental data as well as with those of Reference 2 in Figure 8. It can be seen that both computational results exhibited fair comparison with the experimental data. At x/c=0.75, the present velocity profile compared more favorably with experimental data than that of Reference 2. The velocity profiles obtained using the J-A model [3] also compared favorably with experimental data. The level of agreement with experimental data was the same as the present one. The improvement in the calculated velocity profile is attributed to the turbulence models which yielded better turbulence fields than the W-R model.

The calculated turbulent kinetic energy profiles are compared with experimental data in Figure 9. It can be seen in the figure that the

magnitude and location of the turbulent kinetic energy compared favorably with experimental data. Again, the present turbulence model yielded significantly improved computational result at x/c=0.75. It has been shown in Reference 5 that the near-wall turbulence model can resolve details of the near-wall turbulence including the over-shoot phenomena of the turbulent kinetic energy and the dissipation rate in the region very close to the wall. Considering this fact, it is not fortuitous that the near-wall turbulence model yielded improved turbulent kinetic energy profile at x/c=0.75.

The Reynolds stress profiles at the same axial locations are shown in Figure 10. It can be seen that the present turbulence model under predicted the magnitude of the Reynolds stress. The Reynolds stress profiles presented in Reference 3 also exhibited the same trend as the present results. It has long been argued that the algebraic turbulence models and the k-ϵ turbulence models can not resolve recirculating turbulent flows accurately. The same argument can be applied to the present computational results. However, the flow field in the downstream region of the curved hill did not affect the upstream region significantly and the correct surface pressure distribution and the shock location were obtained in the numerical calculations.

Conclusions

A control-volume based finite difference computation of a turbulent transonic flow using a k-ϵ turbulence model supplemented with a near-wall turbulence model has been presented. It has been shown that the present method was strongly convergent for the high Reynolds number flow with arbitrary geometry and that the method yields significantly accurate

computational results for the transonic flow with the shock wave - turbulent boundary layer interaction. The strongly convergent nature is attributed to the near-wall turbulence model, the pressure-staggered grid layout, and the pressure correction method. The improved computational results are attributed to the near-wall turbulence model.

In the near-wall turbulence model, the turbulent kinetic energy equation was integrated up to the wall and the dissipation rate inside the near-wall region was obtained from an algebraic equation. This approach was found to be more advantageous than the low Reynolds number turbulence models since the stiff dissipation rate equation in the near-wall region need not be solved numerically. In some numerical calculations of turbulent flows, algebraic turbulence models have been preferred over k-ϵ turbulence models to overcome the numerical difficulty originating from the stiff dissipation rate equation [3,36,37]. This difficulty is considerably reduced by using the partially low Reynolds number turbulence models. More importantly, the near-wall turbulence model yielded significantly accurate computational results for the near-wall turbulence field of the shock wave - turbulent boundary layer interaction flow. For the separated flow region at the rear end of the hill, the present turbulence model as well as the J-A model yielded degenerated computational results. The degenerated computational results are attributed to the limited capability of the algebraic turbulence model and the k-ϵ turbulence model to resolve recirculating turbulent flows [8,35]. However, the usefulness of the present turbulence model to solve turbulent flows with a small separated flow region has been demonstrated in this study.

References

1. Bachalo, W.D.; and Johnson, D.A.: An Investigation of Transonic Turbulent Boundary Layer Separation Generated on an Axisymmetric Flow Model. AIAA Paper 79-1479, July 1979.

2. Johnson, D.A.; Horstman, C.C.; and Bachalo, W.D.: Comparison Between Experiment and Prediction for a Transonic Turbulent Separated Flow. AIAA J., vol. 20, no. 6, June 1982, pp. 737-744.

3. Johnson, D.A.: Transonic Separated Flow Prediction with an Eddy-Viscosity/ Reynolds-Stress Closure Model. AIAA J., vol. 25, no. 2, Feb. 1987, pp. 252-259.

4. Kim, S.W.: A Control Volume Based Reynolds Averaged Navier-Stokes Equation Solver Valid at All Flow Velocities. NASA TM- , 1989, to be published.

5. Kim, S.W.: A Near-Wall Turbulence Model and Its Application to Fully Developed Turbulent Channel and Pipe Flows. NASA TM-101399, 1988.

6. Patankar, S.V.; and Shih, T.M.: Numerical Heat Transfer and Fluid Flow. McGraw-Hill, 1980.

7. Gosman, A.D.; and Ideriah, F.J.K.: TEACH-T. Department of Mechanical Engineering, Imperial College, London, 1982.

8. Kline, S.J.; Cantwell, B.J.; and Lilley, G.M., eds.: Complex Turbulent Flows. Vols. 1-3, Thermosciences Division, Mechanical Engineering Dept., Stanford University, 1981.

9. Jones, W.P.; and Whitelaw, J.H.: Calculation Methods for Reacting Turbulent Flows: A Review. Combust. Flame, vol. 48, no. 1, Oct. 1982, pp. 1-26.

10. Beam, R.M.; and Warming, R.F.: An Implicit Factored Scheme for the Compressible Navier-Stokes Equations. AIAA J., vol. 16, no. 4, Apr. 1978, pp. 393-402.

11. MacCormack, R.W.: A Numerical Method for Solving the Equations of Compressible Viscous Flow. AIAA J., vol. 20, no. 9, Sept. 1982, pp. 1275-1281.

12. Rhie, C.M.: A Pressure Based Navier-Stokes Solver Using the Multigrid Method. AIAA Paper 86-0207, Jan. 1986.

13. Karki, K.C.; and Patankar, S.V.: A Pressure Based Calculation Procedure for Viscous Flows at All Speeds in Arbitrary Configurations. AIAA Paper 88-0058, Jan. 1988.

14. Chen, Y.S.: Viscous Flow Computations Using a Second-Order Upwind Differencing Scheme. AIAA Paper 88-0417, Jan. 1988.

15. Maliska, C.R.; and Raithby, G.D.: A Method for Computing Three-Dimensional Flows Using Non-Orthogonal Boundary-Fitted Coordinates. Int. J. Numer. Methods Fluids, vol. 4, no. 6, June 1984, pp. 519-537.

16. Fortin, M.; and Fortin, A.: Newer and Newer Elements for Incompressible Flow. Finite Elements in Fluids, Vol. 6, R.H. Gallagher, et al., eds, J. Wiley and Sons, New York, 1985, pp. 171-187.

17. Vanka, S.P.; Chen, B.C.J.; and Sha, W.T.: A Semi-Implicit Calculation Procedure for Flows Described in Boundary-Fitted Coordinate System. Numer. Heat Trans., vol. 3, no. 1, Jan.-Mar. 1980, pp. 1-19.

18. Raithby, G.D.; and Schneider, G.E.: Numerical Solution of Problems in Incompressible Fluid Flow: Treatment of the Velocity-Pressure Coupling. Numer. Heat Transfer., vol. 2, no. 4, Oct.-Dec. 1979, pp 417-440.

19. Viegas, J.R.; Rubesin, M.W.; and Horstman, C.C.: On the Use of Wall Functions as Boundary Conditions for Two-Dimensional Separated Compressible Flows. AIAA Paper 85-0180, Jan. 1985.

20. Gorski, J.J.: A New Near-Wall Formulation for the Kappa-Epsilon Equations of Turbulence. AIAA Paper 86-0556, Jan. 1986.

21. Amano, R.S.: Development of a Turbulence Near-Wall Model and Its Application to Separated and Reattached Flows. Numer. Heat Transfer, vol. 7, no. 1, Jan.-Mar. 1984, pp. 59-75.

22. Kim, S.W.; and Chen, C.P.: A Finite Element Computation of Complex Turbulent Boundary Layer Flows with a Two-Layer Multiple-Time-Scale Turbulence Model. NASA CR- , 1988.

23. Patel, V.C.; Rodi, W.; and Scheuerer, G.: Turbulence Models for Near-Wall and Low Reynolds Number Flows: A Review, AIAA J., vol. 23, no. 9, Sept. 1985, pp. 1308-1319.

24. Chen, H.C.; and Patel, V.C.: Practical Near-Wall Turbulence Models for Complex Flows Including Separation. AIAA Paper 87-1300, June 1987.

25. Wolfshtein, M.: The Velocity and Temperature Distribution in One-Dimensional Flow with Turbulence Augmentation and Pressure Gradient. Int. J. Heat Mass Trans., vol. 12, no. 3, Mar. 1969, pp. 301-318.

26. Roshko, A.: Structure of Turbulent Shear Flows: A New Look. AIAA J., vol. 14, no. 10, Oct. 1976, pp. 1349.1357,

27. Settles, G.S.; Vas, I.E.; and Bogdonoff, S.M.: Details of a Shock-Separated Turbulent Boundary Layer at a Compression Corner. AIAA J., vol. 14, no. 12, Dec. 1976, pp. 1709-1715.

28. White, F.M.: Viscous Fluid Flow. McGraw-Hill, 1974.

29. Gibson, M.M.; Spalding, D.B.; and Zinser, W.: Boundary-Layer Calculations Using the Hassid-Poreh One-Equation Energy Model. Letters in Heat and Mass Transfer, vol. 5, no. 2, Mar.-Apr. 1978, pp. 73-80.

30. Hassid, S.; and Poreh, M.: A Turbulent Energy Model for Flows with Drag Reduction. J. Fluids Eng., vol. 97, no. 2, June 1975, pp. 234-241.

31. Acharya, M.; and Reynolds, W. C.: Measurements and Predictions of a Fully Developed Turbulent Channel Flow with Imposed Controlled Oscillations. Thermoscience Division, Stanford University, Tech. Report TF-8, 1975.

32. Harlow, F.H.; and Nakayama, P.I.: Transport of Turbulence Energy Decay Rate. LA-3854, 1968.

33. Kim, S.W.; and Chen, Y.S.: A Finite Element Computation of Turbulent Boundary Layer Flows with an Algebraic Stress Turbulence Model. Comput. Methods Appl. Mech. Eng., vol. 66, no. 1, Jan. 1988, pp. 45-63.

34. Kim, S.W.; and Chen, C.P.: A Multiple-Time-Scale Turbulence Model Based on Variable Partitioning of the Turbulent Kinetic Energy Spectrum. To appear in Numer. Heat Trans. 1989. (Also available as NASA CR-179222, 1987 and AIAA Paper 88-0221, 1988).

35. Klebanoff, P.S.: Characteristics of Turbulence in a Boundary Layer with Zero Pressure Gradient. NACA Report 1247, 1955.

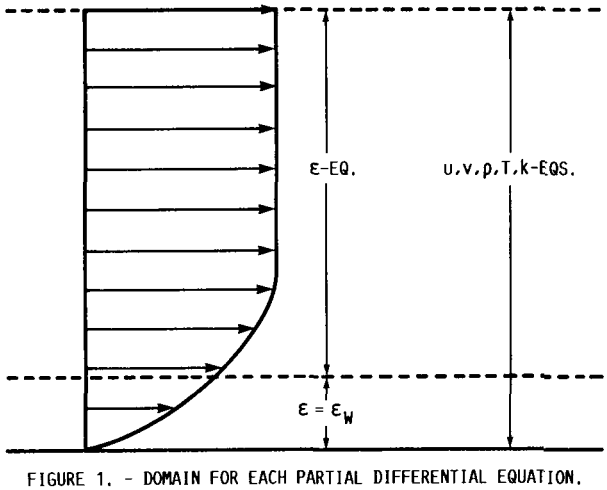

FIGURE 1. - DOMAIN FOR EACH PARTIAL DIFFERENTIAL EQUATION.

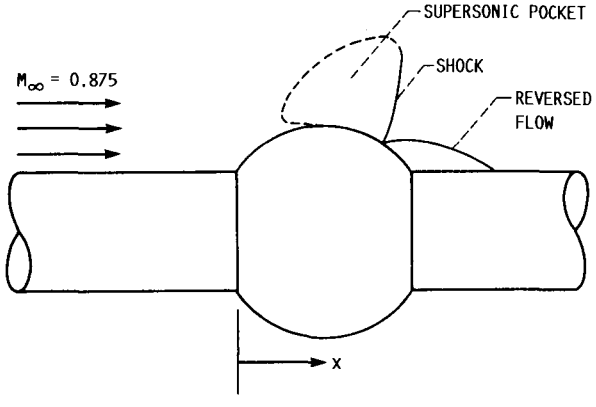

FIGURE 2. - TRANSONIC FLOW OVER AN AXISYMMETRIC CURVED HILL.

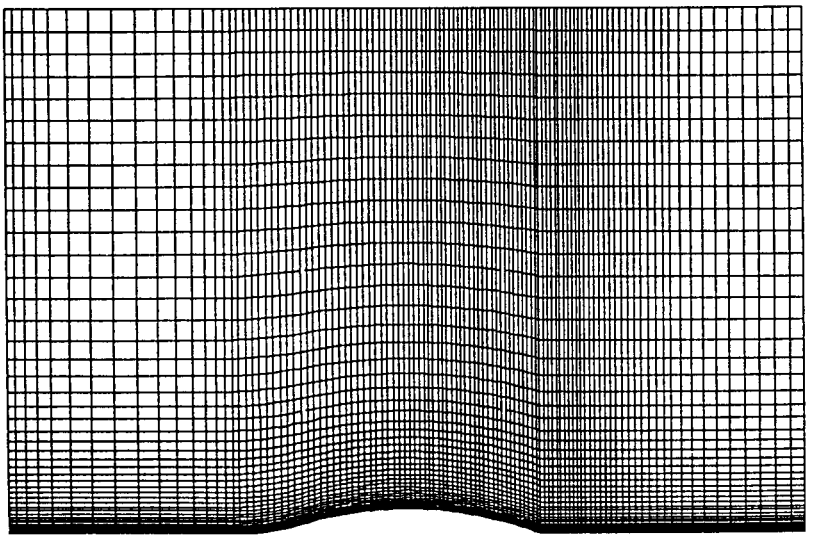

FIGURE 3. - DISCRETIZATION OF THE FLOW DOMAIN (108 x 65 MESH).

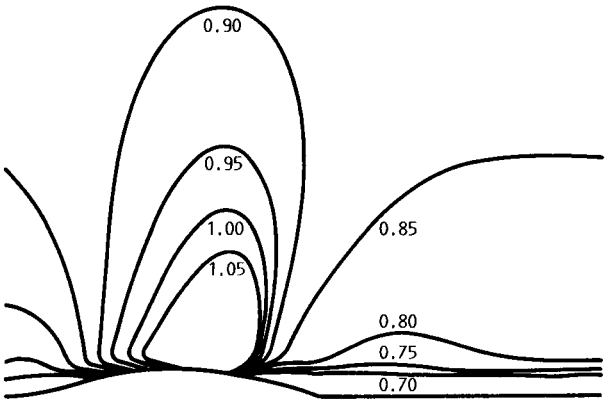

FIGURE 4. - ISO-MACH LINES.

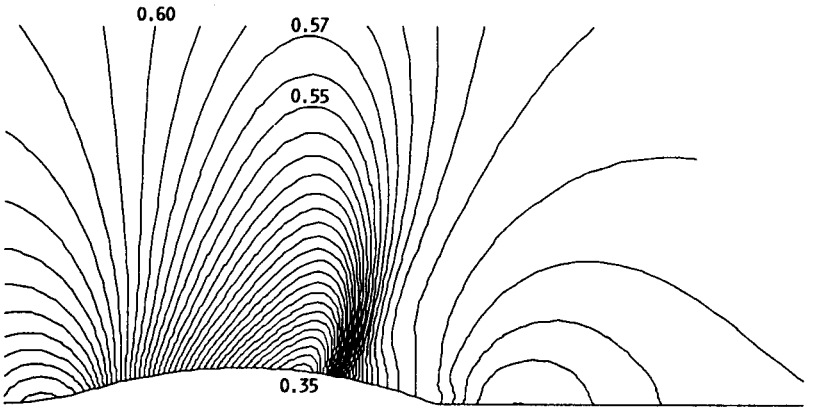

FIGURE 5. - PRESSURE CONTOUR.

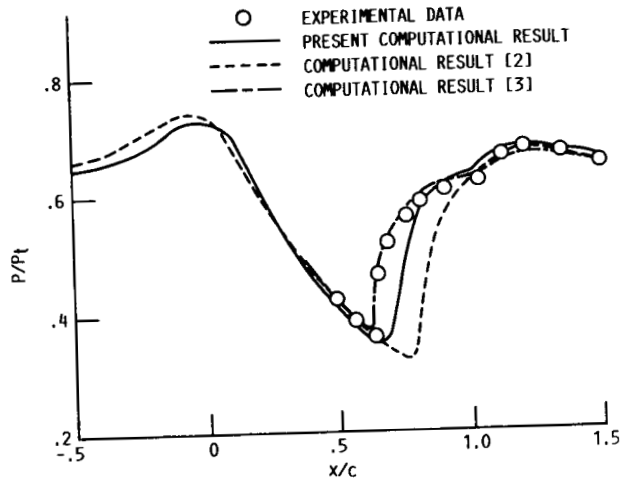

FIGURE 6. - PRESSURE DISTRIBUTION ON THE WALL.

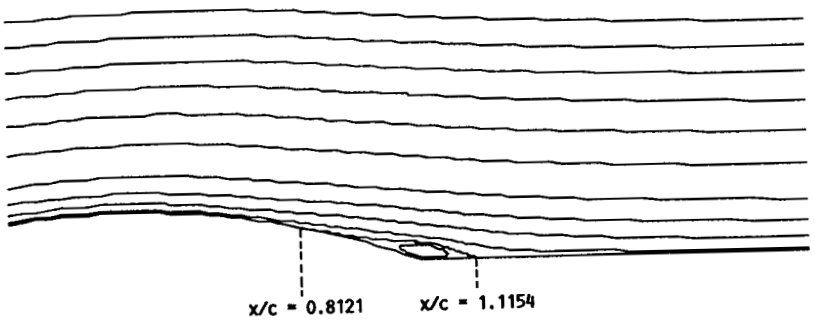

FIGURE 7. - STREAMLINE CONTOUR.

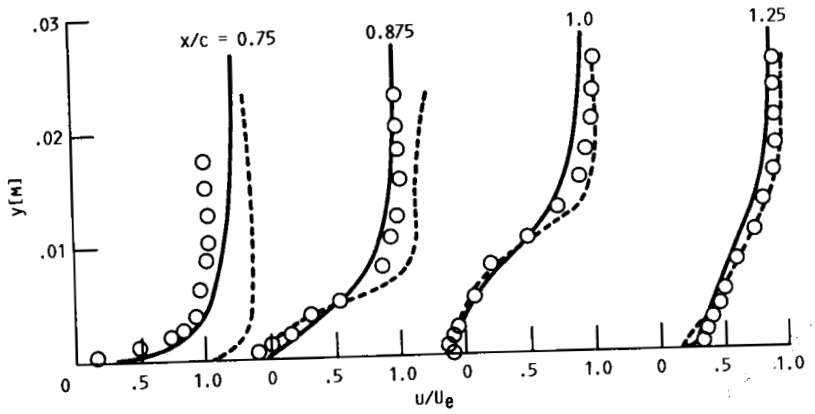

FIGURE 8. - VELOCITY PROFILES, NOTATIONS AS IN FIGURE 6.

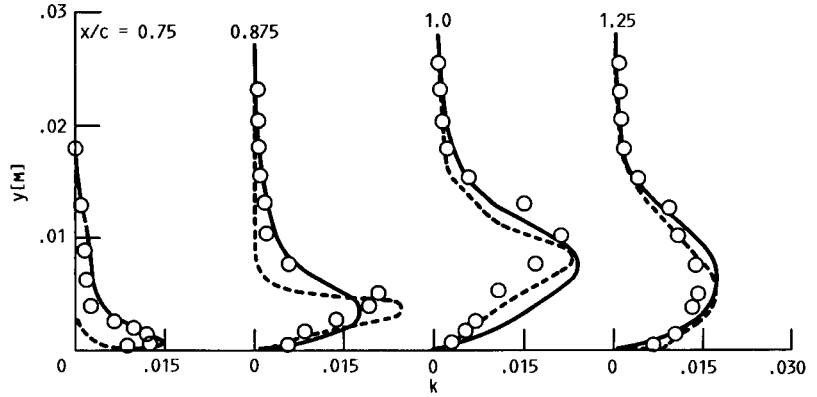

FIGURE 9. - VELOCITY PROFILES, NOTATIONS, AS IN FIGURE 6.

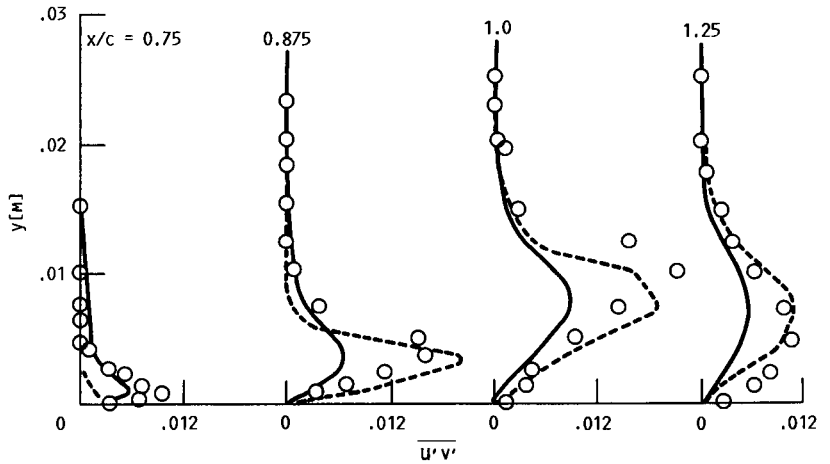

FIGURE 10. - REYNOLDS STRESS PROFILES, NOTATIONS AS IN FIGURE 6.

NASA
National Aeronautics and Space Administration

Report Documentation Page

1. Report No.	2. Government Accession No.	3. Recipient's Catalog No.
NASA TM-101473 ICOMP-89-3		

4. Title and Subtitle

Numerical Computation of Shock Wave—Turbulent Boundary Layer Interaction in Transonic Flow Over an Axisymmetric Curved Hill

5. Report Date
February 1989

6. Performing Organization Code

7. Author(s)
S.-W. Kim

8. Performing Organization Report No.
E-4589

10. Work Unit No.
505-62-21

9. Performing Organization Name and Address
National Aeronautics and Space Administration
Lewis Research Center
Cleveland, Ohio 44135-3191

11. Contract or Grant No.

13. Type of Report and Period Covered
Technical Memorandum

12. Sponsoring Agency Name and Address
National Aeronautics and Space Administration
Washington, D.C. 20546-0001

14. Sponsoring Agency Code

15. Supplementary Notes

S.-W. Kim, Institute for Computational Mechanics in Propulsion (work funded under Space Act Agreement C99066G).

16. Abstract

A control-volume based finite difference computation of a turbulent transonic flow over an axisymmetric curved hill is presented. The numerical method is based on the SIMPLE algorithm, and hence the conservation of mass equation is replaced by a pressure correction equation for compressible flows. The turbulence is described by a k-ϵ turbulence model supplemented by a near-wall turbulence model. In the method, the dissipation rate in the region very close to the wall is obtained from an algebraic equation and that for the rest of the flow domain is obtained by solving a partial differential equation for the dissipation rate. The other flow equations are integrated up to the wall. It is shown that the present turbulence model yields the correct location of the compression shock. The other computational results are also in good agreement with experimental data.

17. Key Words (Suggested by Author(s))
Transonic flow
Near-wall turbulence model

18. Distribution Statement
Unclassified – Unlimited
Subject Category 34

19. Security Classif. (of this report)	20. Security Classif. (of this page)	21. No of pages	22. Price*
Unclassified	Unclassified	30	A03

*For sale by the National Technical Information Service, Springfield, Virginia 22161